Current **A**pplied **S**cience and **T**echnology e-ISSN: 2586-9396

Curr. Appl. Sci. Technol. ….., Vol... (No...), e0267791

Research article

Utilization of Bottom Ash from Power Plants as Backfill Material for Surface Coal Mines with Enhanced Carbon Dioxide Capture and Storage Capabilities

Pintunicha Pongsena[1], Matika Buaphian[1], Nutdanai Srisuk[1], Bunlang Mansanit[1], Manoon Masniyom[1], Matthana Khangkhamano[1,2] and Naruemol Saoanunt[1,2]*

[1]Department of Mining and Materials Engineering, Faculty of Engineering, Prince of Songkla University, Songkhla, Thailand
[2]Center for Sustainable and Advanced Materials (CSAM), Faculty of Engineering, Prince of Songkla University, Songkhla, Thailand

Received: 29 May 2025, Revised: 12 September 2025, Accepted: 14 September 2025, Published:16 January 2026

Abstract

In response to the growing need for sustainable mine reclamation, this study investigates the use of bottom ash, a byproduct of coal or lignite combustion, as a component in backfill materials for surface mining. The study focuses on evaluating the CO_2 absorption capacity and mechanical strength properties of mixtures containing varying ratios of bottom ash and smectite. Composite backfill material strength was assessed through unconfined compressive strength (UCS) and direct shear tests. The mixture with a bottom ash to smectite ratio of 30:70 exhibited the highest UCS across all moisture levels, with a peak value of 139 kPa at 10% water content. At this condition, the mixture also showed a cohesion of 17.06 kPa, an internal friction angle of 31.2°, and a shear strength of 25.32 kPa. Based on these results, samples at 10% water content were selected for CO_2 absorption testing across different bottom ash–smectite ratios. The 10:90 ratio demonstrated the highest CO_2 absorption capacity at 3.16 mg/g, with a decreasing trend observed as the proportion of bottom ash increased. These findings suggest that bottom ash–smectite mixtures can be optimized to achieve both pit wall stability and enhanced carbon sequestration, supporting their use as sustainable backfill materials in mine reclamation.

Keywords: bottom ash; mine backfill material; CO_2 absorption; waste utilization; lignite byproducts; surface coal mines

*Corresponding author: E-mail: naruemol.sao@psu.ac.th
https://doi.org/10.55003/cast.2026.267791

1. Introduction

In Thailand, bottom ash management remains a pressing issue. Most of the ash is landfilled or stockpiled near power plants without adequate containment or long-term monitoring, leading to concerns about groundwater contamination and soil degradation (Pipatmanomai et al., 2009). The lack of standardized treatment protocols and regulatory oversight has hindered efforts to reuse bottom ash in construction or environmental applications. Although bottom ash has potential for beneficial reuse, its chemical instability and heavy metal content limit its safe deployment without further modification.

Bottom ash, a solid residue generated from the combustion of coal and biomass in thermal power plants, represents a significant waste stream in Thailand's energy sector. Bottom ash is a course, granular residue that settles at the base of boilers and is typically composed of a heterogeneous mixture of silicon dioxide (SiO_2), aluminum oxide (Al_2O_3), iron oxide (Fe_2O_3), calcium oxide (CaO), and magnesium oxide (MgO), along with residual carbon and leachable heavy metals that pose environmental risks if not properly managed (Jiarawattananon et al., 2019). Its physical characteristics include high porosity (40-60%), variable particle sizes ranging from 0.1 to 50 mm, and a bulk density of approximately 800-1200 kg/m³ (Singh & Siddique, 2013; Ingold et al., 2024). These properties contribute to its high-water absorption and free-draining behavior, making it potentially useful in geotechnical applications.

To address these challenges, this research has been focused on developing composite materials that combine bottom ash with naturally occurring minerals to enhance its environmental performance. One promising approach involves blending bottom ash with smectite clay, a group of phyllosilicate minerals known for their high cation exchange capacity (CEC), swelling behavior, and strong affinity for heavy metals and organic pollutants. Smectite's layered structure and abundant active sites enable it to adsorb contaminants through ion exchange, surface complexation, and interlayer intercalation. Studies have shown that modified smectite clays can effectively remove heavy metals such as Pb, Cd, and As from aqueous solutions, making them suitable for immobilizing hazardous elements in bottom ash composites (Vishwakarma & Shukla, 2024; Wang et al., 2024).

Beyond its role in heavy metal adsorption, smectite also offers potential for carbon dioxide (CO_2) capture and geological storage. The interlayer spaces of smectite can accommodate CO_2 molecules through physisorption and carbonate formation, allowing for long-term retention under subsurface conditions (Câmara et al., 2023; Wang et al., 2024). When exposed to CO_2, smectite undergoes swelling and stress-strain changes that can help seal fractures and reduce permeability in geological formations (War et al., 2023). This behavior is particularly valuable in mining environments, where CO_2 sequestration and structural stability are critical concerns. By incorporating smectite into bottom ash composites, researchers aim to create multifunctional materials capable of both environmental remediation and geotechnical reinforcement.

The integration of bottom ash and smectite into a single engineered material offers several advantages. First, it provides a sustainable pathway for managing bottom ash waste, transforming a problematic industrial by-product into a value-added resource, as shown in early studies on incineration ash reuse for subbase construction (Fujikawa et al., 2019). Second, it leverages the natural adsorption capabilities of smectite to mitigate environmental risks associated with heavy metal contamination (Franco et al., 2014). Third, it contributes to climate change mitigation by facilitating CO_2 sequestration in mining environments (Kim & Lee, 2017). Finally, it enhances the geotechnical stability, reducing

the risk of collapse and improving safety for workers and surrounding communities (Fujikawa et al., 2019).

This study investigates the synthesis and characterization of a novel composite material derived from bottom ash and smectite clay, with the goal of developing an integrated solution for CO_2 storage in mining operations. The research evaluates the composite's potential for CO_2 absorption. Additionally, the mechanical properties of the composite including compressive strength and shear strength are analyzed to determine its suitability for stabilizing mine walls and preventing structural failure.

2. Materials and Methods

2.1 Physical characteristic test

Bottom ash samples used in this study were collected from the Mae Moh coal-fired power plant in Lampang Province, Thailand, as illustrated in Figure 1(A). Microscopic observation of the bottom ash was conducted using an optical microscope Carl Zeiss Axio Scope.A1 at 20× magnification. Scanning electron microscopy (SEM) using a SU3900 model was also employed to examine particle morphology and surface characteristics.

To analyze the physical characteristics of the bottom ash, sieve analysis was performed in accordance with the ASTM D 422 standards (ASTM, 2007) to determine particle size distribution. Particle shape classification was conducted using the Power Roundness Scale (Power, 1953).

Water content of bottom ash was measured following the ASTM D 2216-98 procedures (ASTM, 2017). Specific gravity and water absorption tests were carried out according to the ASTM C 128 standards (ASTM, 2023) to evaluate the density and absorption properties of the bottom ash material.

Smectite belongs to the group of clay minerals in the phyllosilicate. Key minerals in this group include montmorillonite, beidellite, and nontronite. Due to its extremely fine particle size and high-water absorption and expansion capacity, the smectite exhibits unique properties such as swelling ability and ion exchange capacity, which significantly influence the physical, mechanical, and chemical properties of clay (Pusch & Yong, 2006).

In this study, the smectite sample used appeared as a fine powder in white, gray, or light green, resembling talc or finely ground limestone. Particle morphology and surface characteristics of the smectite were examined using scanning electron microscopy (SEM, model SU3900).

2.2 Chemical characteristic test

X-ray diffraction (XRD) analysis of the bottom ash and smectite samples was performed using an Empyrean diffractometer to identify the crystalline phases present in the material. The analysis was conducted by comparing the 2θ peak positions with standard entries from the Joint Committee on Powder Diffraction Standards (JCPDS).

Chemical composition of the bottom ash and smectite samples was determined using X-ray Fluorescence spectroscopy (XRF ZETIUM), with results expressed in terms of weight percentages of various oxides, including major, minor, and trace components.

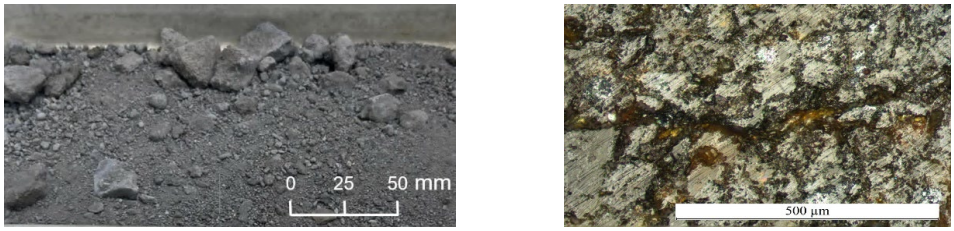

Figure 1. (A) Bottom ash sample collected from the Mae Moh power plant, Lampang, Thailand. (B) Microscopic view of the bottom ash sample captured using an optical microscope at 20X magnification

Loss on Ignition (LOI) of both samples was measured using a simultaneous thermal analyzer (STA8000) to evaluate the presence of volatile substances and thermally unstable compounds.

2.3 Preparation of backfill material samples

The purpose of sample preparation was to conduct compaction, unconfined compressive strength (UCS), and CO_2 absorption tests. For all 3 tests, bottom ash was mixed with smectite clay in the following ratios: 90:10, 80:20, 70:30, 50:50, 30:70, and 10:90. Each bottom ash–smectite mixture was prepared with water contents of 4%, 7%, and 10%. Sample preparation for the compaction test followed the ASTM D698 standard (ASTM, 2021), using a 4-inch diameter mold and 5.5-pound hammer. The samples were compacted in 3 layers with 25 blows per layer. For the UCS test, the same mixing ratios were used as those in the compaction test. Sample preparation followed the ASTM D2166-06 standards (ASTM, 2010a), forming cylindrical specimens with a minimum diameter of 30 mm (1.3 inches). The maximum particle size of the material could not exceed 1/10 of the sample diameter, and the sample height was set between 2 and 2.5 times its diameter. For this study, the specimens were prepared with a diameter of 40 mm and a height of 80 mm, with 5 specimens per ratio, as shown in Figure 2. After molding, the samples were cured for 7 days before the UCS test was conducted. For the CO_2 absorption test, the sample preparation followed the same method as the UCS test, with compacted cylindrical specimens that were cured for 7 days before testing. To determine the optimal composition of the backfill materials, 6 different mixing ratios were evaluated, each mixed with a water content of 4%, 7%, and 10%, respectively. The investigated bottom ash to smectite mixing ratios were as follows: 90:10, 80:20, 70:30, 50:50, 30:70, and 10:90.

Figure 2. Composite material sample compacted into cylindrical compacts (40×80 mm)

2.4 Mechanical property test and CO_2 absorption test

2.4.1 Compaction test

In this study, bottom ash was mixed with smectite clay at weight ratios of 90:10, 80:20, 70:30, 50:50, 30:70, and 10:90. Each mixture was prepared by blending the designated proportions of bottom ash and smectite, followed by addition of water at 4%, 7%, and 10% by total dry weight, using the same mixing procedure described in Section 2.3. The compaction test was conducted following the ASTM D698 standard (ASTM, 2021) using the standard compaction test method. A 4-inch diameter mold and 5.5-pound hammer were used to compact the material in 3 layers, with 25 blows per layer. Each ratio was tested 3 times to ensure accuracy and reliability. After compaction, the samples were weighed and data recorded, and the data were used to calculate the optimum moisture content (O.M.C.), which represents the moisture level that results in the highest material density.

2.4.2 Unconfined compressive strength test

The unconfined compressive strength (UCS) test was conducted using backfill material mixed in the same proportions as those employed in the compaction test. The procedure followed the ASTM D2166-06 standard (ASTM, 2010a), which specifies the method for UCS testing under undrained conditions. For specimen preparation, the mixed materials were compacted into cylindrical molds measuring 40 × 80 mm. Each mix ratio was represented by five specimens, which were cured for a period of seven days prior to testing. UCS measurements were performed using a 5-ton compression machine manufactured by Wyke Farrance ENG. LTD, Slough, England.

2.4.3 Direct shear test

The shear strength test in this study involved mixing bottom ash with smectite in the same ratio as that used in the compaction test. The apparatus used for the shear strength test, a direct shear testing machine (Controls, model T 206-010), was operated in accordance with the ASTM D 3080 standards (ASTM, 2020). Three loading levels were applied during the testing process: 1 kg, 3 kg, and 5 kg. The results obtained from the test are presented as relationships in Figures 10. The results of this test can be calculated the cohesion force (c), friction angles (ϕ) and the shear strength (τ) using the Mohr-Coulomb criteria.

2.4.4 CO_2 absorption test

The CO_2 absorption test for the backfill material samples mixed with bottom ash and smectite clay was designed using cylindrical samples (40 × 80 mm), similar to those used in the unconfined compressive strength test. The water content of the samples used for this test was 10%, and they were cured for seven days. This was based on the results of the unconfined compressive strength test, which indicated that samples with 10% moisture content could retain their shape and withstand strength better than those with other moisture contents. The CO_2 used in this test was 100% pure laboratory-grade carbon dioxide (≥99.99%) to ensure consistency and eliminate interference from other gases. The CO_2 absorption test began by placing the prepared samples in a sealed container, introducing CO_2 gas at a flow rate of 15 litres per minute for 2 min, and allowing the samples to absorb the gas for an additional minute without further CO_2 injection. Subsequently, the

sample weight was measured using a precision balance with three decimal places, and the recorded weight change was noted. This process was repeated until the weight stabilized or decreased.

3. Results and Discussion

3.1 Physical characteristics

3.1.1 Bottom ash

The bottom ash samples collected from the Mae Moh coal-fired power plant in Lampang Province, Thailand, exhibited distinct physical characteristics that were critical for evaluating their potential reuse in backfill material applications. Optical microscopy at 20× magnification revealed a highly porous structure with abundant voids, as shown in Figure 1(B), while SEM analysis (Figure 3) confirmed the presence of large, irregular particles, including spherical agglomerates and porous fragments. Figure 4 presents the particle size distribution of the bottom ash, which was classified as gravel, with particle sizes ranging from coarse sand to fine gravel. According to the Unified Soil Classification System (ASTM, 2010b), the calculation of the coefficient of uniformity (C_U = 5.68), and the coefficient of curvature (C_C =0.58) indicate that the material is poorly graded (GP). Additionally, the particle morphology was characterized as angular to very angular, based on the Power Roundness Scale (Power, 1953). These characteristics can enhance shear strength but may also lead to increased water absorption and reduced durability (Siddique, 2008). Water content analysis, performed according to ASTM D 2216 (ASTM, 2010a), yielded a value of 16.50%, indicating moderate hygroscopic behavior. Specific gravity and water absorption tests (ASTM C 128) (ASTM, 2023) revealed a dry specific gravity of 2.07, saturated surface dry specific gravity of 2.33, and apparent specific gravity of 2.77. The water absorption capacity of 12.12% was notably high, which aligned with observations by Ksaibati and Sayiri (2006), who reported that bottom ash tended to exhibit elevated absorption rates due to its porous microstructure.

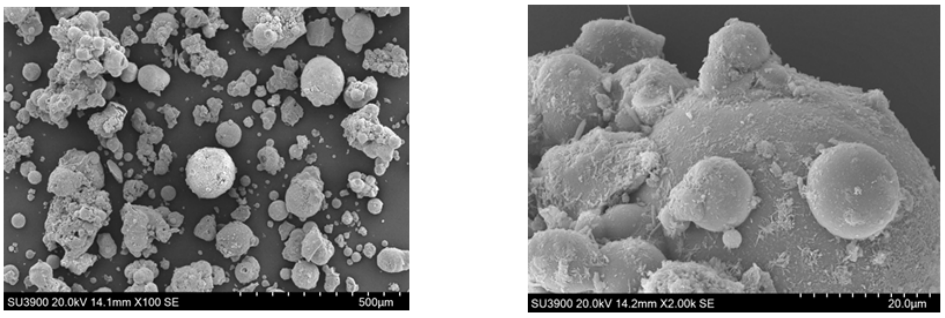

(A) (B)

Figure 3. Particle characteristics of the bottom ash sample from Mae Moh power plant analyzed using scanning electron microscopy (SEM), where (A) represents as-received bottom ash and (B) represents ground bottom ash.

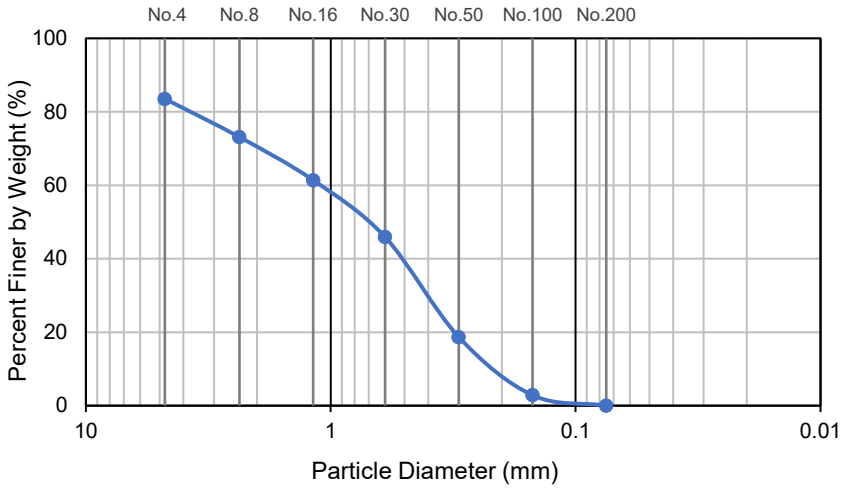

Figure 4. Relationship between particle diameter and the percent finer by weight, showing the particle size distribution of bottom ash with a poorly graded gravel profile (GP) based on USCS classification.

3.1.2 Smectite

The smectite sample appeared as a fine powder in white, gray, or light green, resembling talc or finely ground limestone. SEM analysis revealed a rough texture with high porosity, as shown in Figure 5(A). The mineral surface was composed of numerous overlapping small plate-like structures, as illustrated in Figure 5(B).

The high porosity and surface roughness observed in the SEM analysis of the smectite sample suggest a favorable morphology for gas adsorption. Supporting this observation, Michels et al. (2015) reported that smectite group of clay minerals with a layered structure can intercalate CO_2 molecules into their interlayer spaces. The interlayer cations play a key role in regulating the adsorption and release of CO_2, making these clays a cost-effective and environmentally friendly option for carbon capture applications.

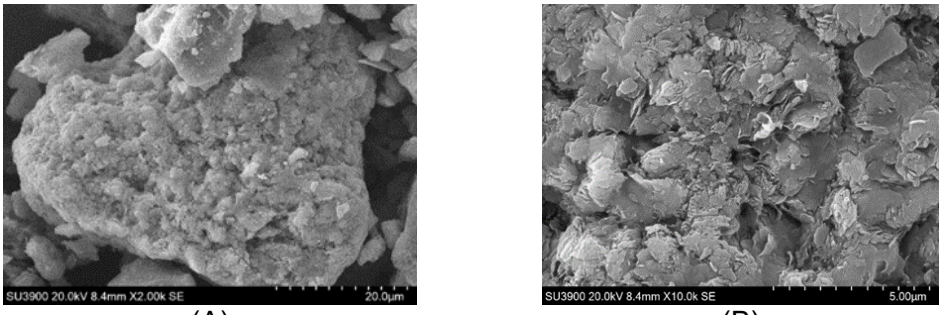

(A) (B)

Figure 5. (A) Particle characteristics and (B) surface morphology of the smectite sample examined using scanning electron microscopy (SEM)

3.2 Chemical characteristics

3.2.1 Bottom ash

Figure 6 shows that the bottom ash sample contained three major crystalline phases identified by their 2θ peak positions and matched with standard JCPDS entries: Diopside ($Ca(Mg,Al)(Si,Al)_2O_6$; JCPDS 00-041-1370) at 66%, Akermanite ($Ca_2(Al_{0.46}Mg_{0.54})((Al_{0.23}Si_{0.77})_2O_7)$; JCPDS 01-076-2633) at 24%, and Quartz (SiO_2; JCPDS 01-087-2096) at 10%. These phases were identified based on their 2θ peak positions and matched with standard entries from the Joint Committee on Powder Diffraction Standards (JCPDS). Diopside, a calcium magnesium silicate, is known for its high mechanical strength and chemical durability, making it a key contributor to the structural integrity of the bottom ash matrix (Levien et al., 1979). Akermanite, a melilite-group mineral, has been associated with enhanced bonding properties and potential CO_2 adsorption capabilities due to its open crystal framework and reactive surface sites (Ardit et al., 2012). Quartz, although present in smaller quantities, reinforces the overall rigidity and thermal stability of the material (Götze & Möckel, 2012).

Table 1 presents the chemical composition of the bottom ash sample, expressed as weight percentages of various oxides. The predominant oxides were SiO_2 (30.63%) and CaO (28.73%), indicating silica and calcium oxide as the major constituents. Significant amounts of Fe_2O_3 (18.16%) and Al_2O_3 (12.72%) were also present, potentially influencing the material's physical and chemical behavior. Minor oxides such as MgO, K_2O, Na_2O, and SO_3 were found in quantities below 3%, while trace oxides (<1%) included TiO_2, P_2O_5, BaO, SrO, MnO_2, ZrO_2, Cr_2O_3, Rb_2O, ZnO, As_2O_3, and Y_2O_3. The loss on ignition (LOI) value was measured at 1.65%.

The chemical composition of bottom ash sample determined by XRF analysis further supports the mineralogical findings. The predominant oxides, SiO_2 and CaO reflect the silicate and calcium-rich nature of the sample. The presence of Fe_2O_3 and Al_2O_3 suggests potential for redox activity and structural reinforcement. Minor oxides such as MgO, K_2O, Na_2O, and SO_3 (<3%) contribute to the material's reactivity and may influence its behavior under environmental conditions. Trace elements, including TiO_2, P_2O_5, BaO, and others (<1%), indicate the complex geochemical background of the ash. The presence of CO_2 and H_2O suggests residual volatile compounds or moisture content in the sample. The measured LOI of 1.65% suggests minimal organic or volatile content, affirming the sample's thermal stability.

3.2.2 Smectite

The smectite sample exhibited a layered silicate structure typical of phyllosilicate clays, as confirmed by XRD analysis. Figure 7, which shows the XRD analysis of the smectite sample, revealed 3 major crystalline phases, identified by their 2θ peak positions and matched with standard entries from the Joint Committee on Powder Diffraction Standards (JCPDS) database. The first phase is sodium aluminum silicate ($NaAlSi_3O_8$; JCPDS No. 01-071-1151). The second phase is montmorillonite-calcián ($Ca_{0.2}(Al,Mg)_2Si_4O_{10}(OH)_2 \cdot xH_2O$; JCPDS No. 00-058-2007). The third phase, fluorophlogopite-1M, syn ($KMg_3(Si_3Al)O_{10}F_2$; JCPDS No. 00-016-0344), contains fluoride within its silicate structure. Sodium aluminum silicate contributes to the mechanical strength and may enhance the material's gas adsorption potential due to its open framework. Montmorillonite-calcián, a key member of the smectite group, is renowned for its high swelling capacity, ion exchange properties, and environmental applicability, particularly in CO_2 capture and heavy metal remediation. The presence of fluorophlogopite, though possibly a result of sample contamination or transformation, introduces fluoride into the structure, which may alter surface reactivity and adsorption behavior.

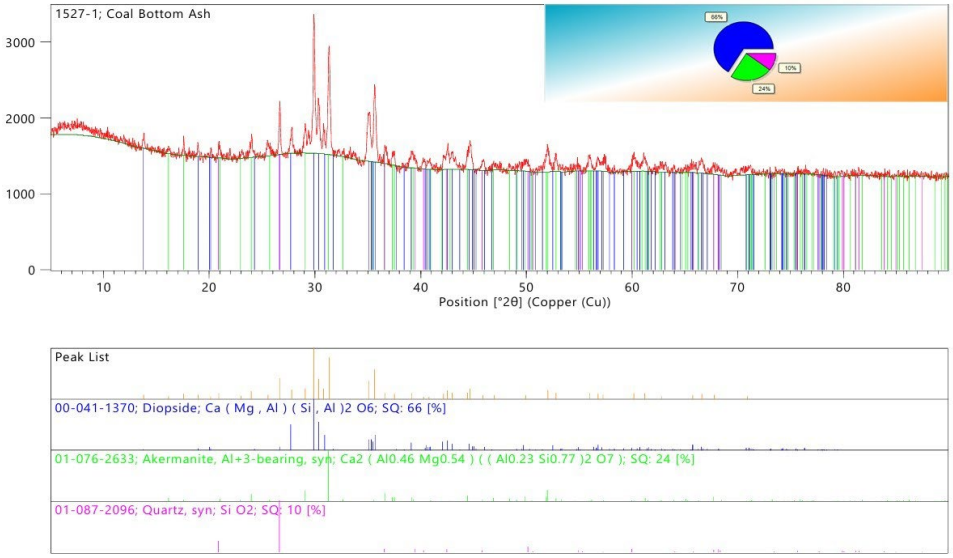

Figure 6. XRD analysis results showing peak positions and crystalline structure of bottom ash sample

Table 1. Chemical composition of the bottom ash sample from XRF analysis

Oxide Composition	% by Weight	Oxide Composition	% by Weight
CaO	28.73	TiO_2	0.40
SiO_2	30.63	P_2O_5	0.31
Fe_2O_3	18.16	BaO	0.15
Al_2O_3	12.72	SrO	0.16
K_2O	1.79	MnO_2	0.21
MgO	2.06	ZrO_2	0.04
SO_3	2.86	Cr_2O_3	0.03
Na_2O	0.79	Rb_2O	0.015
N_2O_5	1.17	ZnO	0.014
CO_2	0.75	As_2O_3	0.008
H_2O	0.20	LOI	1.65

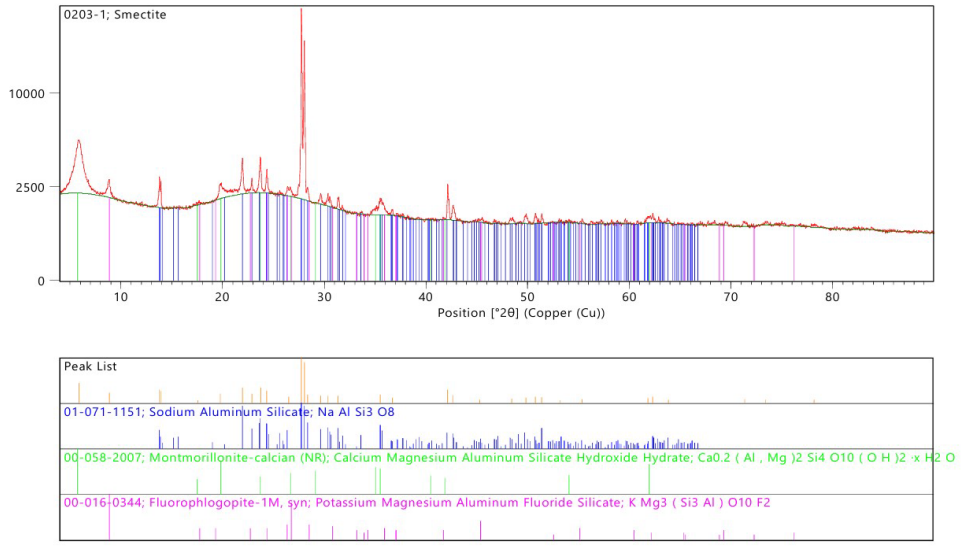

Figure 7. XRD analysis results showing peak positions and crystalline structure of the smectite sample

The chemical composition of the smectite sample was determined using XRF analysis, and the results are presented in Table 2. The data reveal that the sample is predominantly composed of silica (SiO_2), which constitutes 71.74% by weight, indicating a silicate-rich mineral structure typical of smectite clays. The second most abundant oxide is alumina (Al_2O_3) at 15.58%, reflecting the presence of aluminum in the clay matrix. Potassium oxide (K_2O, 4.33%), iron oxide (Fe_2O_3, 2.75%), sodium oxide (Na_2O, 1.92%), calcium oxide (CaO, 1.78%), and magnesium oxide (MgO, 1.13%) are present in moderate amounts, supporting the mineral's swelling behavior and structural stability. Minor oxides such as titanium dioxide (TiO_2, 0.395%), chlorine (Cl, 0.089%), manganese oxide (MnO, 0.052%), and others including zirconia (ZrO_2), barium oxide (BaO), sulfur trioxide (SO_3), strontium oxide (SrO), rubidium oxide (Rb_2O), phosphorus pentoxide (P_2O_5), zinc oxide (ZnO), yttrium oxide (Y_2O_3), and niobium pentoxide (Nb_2O_5) are present in trace amounts (each <0.05%). These values confirm the dominance of the silicate and alumina phases, which are essential for the layered structure and cation exchange capacity of smectite, while the trace oxides reflect the mineral's complex geochemical signature. Additionally, the loss on ignition (LOI) value was measured at 0.73%, indicating low volatile content consistent with the mineral's thermal resilience.

3.3 Mechanical properties

3.3.1 Optimum moisture content (O.M.C.)

The results of the compaction test (Figure 8) show that for all backfill material ratios, the density increased as the moisture content increased. This study used water content of 4%, 7%, and 10%. At 4% water content, the highest dry density or optimum moisture content (O.M.C.) was 1.50 g/cm³ at a 50:50 bottom ash to smectite ratio, whereas the lowest was 1.41 g/cm³ at a 10:90 ratio. At 7% water content, the highest dry density was 1.54 g/cm³ at

50:50, while the lowest was 1.47 g/cm³ at 10:90 ratio. At 10% moisture, the highest dry density was 1.57 g/cm³ at 50:50, while the lowest was 1.49 g/cm³ at 10:90 ratio. The maximum density recorded was 1.57 g/cm³ at 50:50 with 10% water content, whereas the minimum was 1.41 g/cm³ at 10:90 with 4% water content.

Table 2. Chemical compositions of the smectite sample from XRF analysis

Oxide Composition	% by Weight	Oxide Composition	% by Weight
SiO_2	71.74	ZrO_2	0.041
Al_2O_3	15.58	BaO	0.028
K_2O	4.33	SO_3	0.031
Fe_2O_3	2.75	SrO	0.024
Na_2O	1.92	Rb_2O	0.016
CaO	1.78	P_2O_5	0.027
MgO	1.13	ZnO	0.006
TiO_2	0.395	Y_2O_3	0.004
Cl	0.089	Nb_2O_5	0.007
MnO	0.052	LOI	0.73

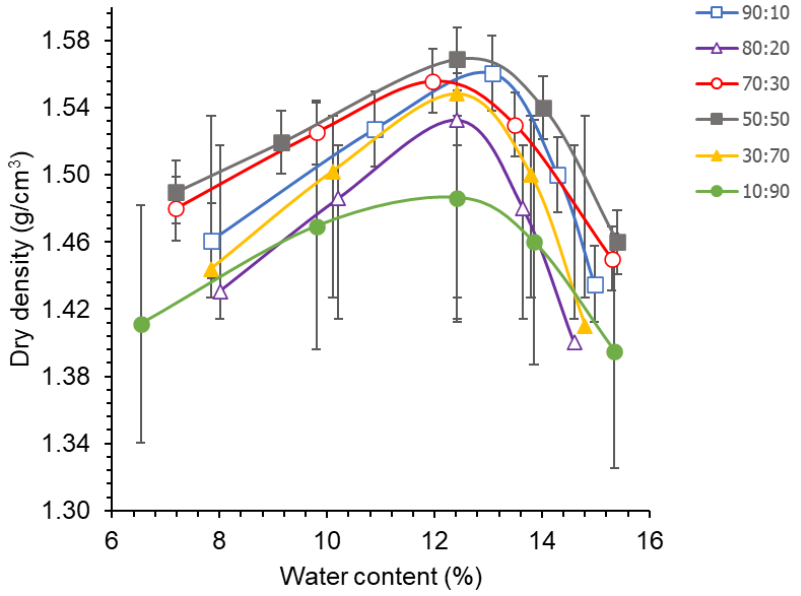

Figure 8. Compaction curves for bottom ash mixed with smectite clay

3.3.2 Unconfined compressive strength

The unconfined compressive strength (UCS) test was conducted to determine the compressive strength of each backfill material ratio, and the test results are shown in Figure 9. At 4% water content, the highest UCS was 112.317 kPa at a 30:70 ratio, and the lowest was 73.058 kPa at 90:10. At 7% water content, the highest UCS was 135.875 kPa at 10:90 and the lowest was 73.077 kPa at 90:10. At 10% water content, the highest UCS was 138.560 kPa at 30:70, and the lowest was 81.603 kPa at 70:30. The maximum compressive strength recorded was 138.560 kPa at 30:70 with 10% water content, whereas the minimum was 73.058 kPa at 90:10 with 4% water content.

The results of the mechanical strength property testing indicated that increasing the proportion of smectite in the bottom ash mixture improved the compressive strength. This is because smectite clay functions as a cementing material with low swelling properties, providing stronger interparticle cohesion than bottom ash alone. Consequently, the material exhibited greater strength when subjected to compressive forces. These findings align with the research of Scherb et al. (2024), which demonstrated that smectite clay acts as a binding material due to its layered structure, which increases its specific surface area, enhancing chemical reactions and adhesion between particles.

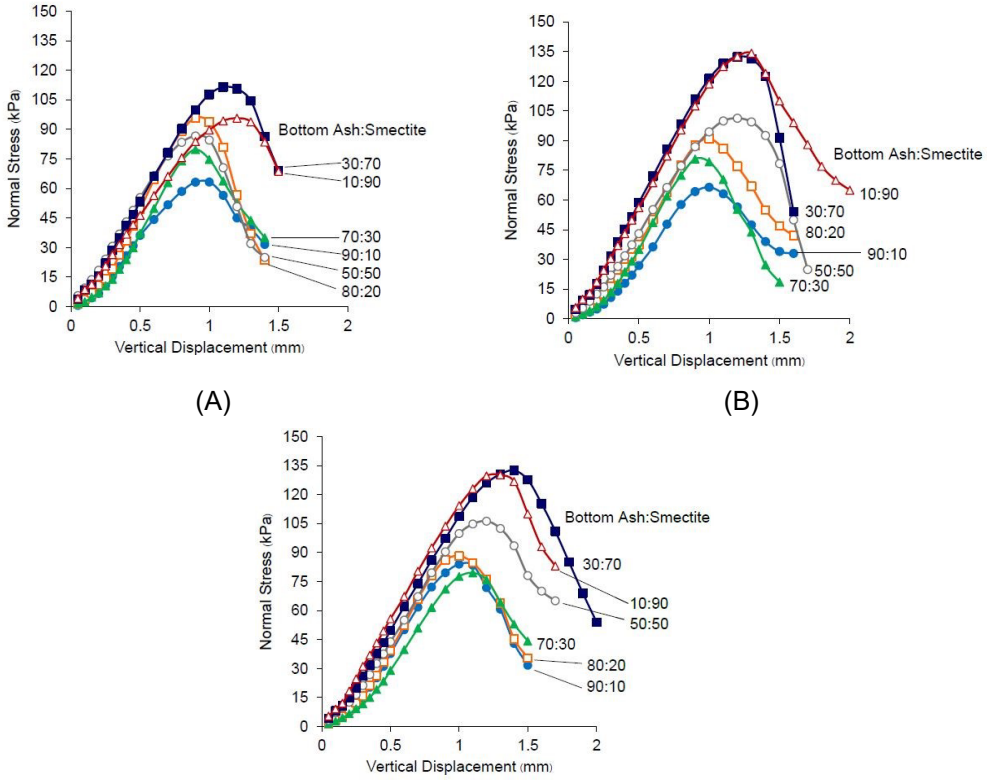

Figure 9. Relationship between vertical compressive stress and vertical displacement of the ash sample mixed with smectite and (a) 4% water (b) 7% water and (c) 10% water

3.3.3 Cohesion, internal friction angle and shear strength

Figure 10 and Table 3 present the results of the direct shear test conducted on backfill material samples composed of varying ratios of bottom ash and smectite clay, with water contents of 4%, 7%, and 10%. The Table includes 3 key mechanical parameters; cohesion (c), internal friction angle (ϕ), and shear strength (τ). These values were calculated using the Mohr-Coulomb failure criterion.

The 90:10 bottom ash to smectite ratio showed high cohesion and friction angle at 4% water content (c = 18.94 kPa, ϕ = 72.6°), resulting in a high shear strength of 64.39 kPa. The 30:70 ratio at 10% water content had moderate cohesion (17.06 kPa) and friction angle (31.2°), yielding a shear strength of 25.32 kPa. The 10:90 ratio, which contains the highest smectite content, showed lower shear strength at all moisture levels compared to other ratios, despite having relatively high cohesion at 4% water content.

Increasing water content generally reduces the internal friction angle, which was expected due to the lubricating effect of water on particle interaction. However, cohesion values fluctuated depending on the mix ratio, indicating that smectite's swelling behavior and bonding capacity played a significant role in interparticle cohesion. The 30:70 ratio at 10% water content appeared to offer a balanced combination of cohesion and friction angle, making it suitable for applications requiring both structural stability and moderate shear resistance. The 90:10 ratio at 4% water content provided the highest shear strength.

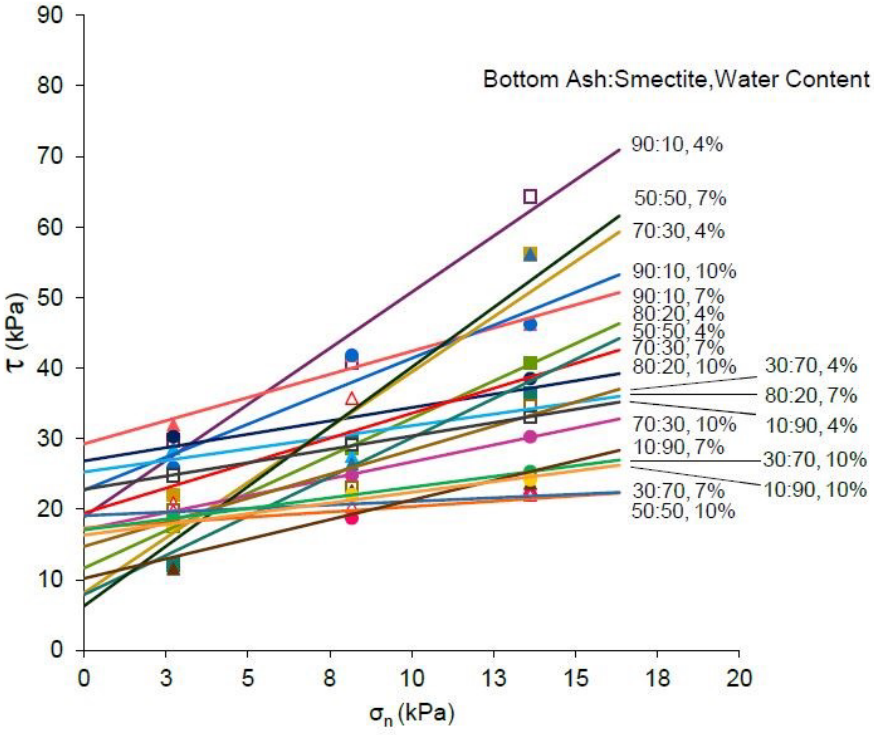

Figure 10. Relationship between shear stress and normal stress of bottom ash mixed with smectite and water at varying ratios following Morh-Coulomb criteria

Table 3. The cohesion force (c) friction angles (ϕ) and the shear strength (τ) for each mixing ratio of the backfill material samples

Ratio	Water Content 4%			Water Content 7%			Water Content 10%		
	c (kPa)	ϕ (°)	τ (kPa)	c (kPa)	ϕ (°)	τ (kPa)	c (kPa)	ϕ (°)	τ (kPa)
90:10	18.94	72.6	64.39	29.26	52.7	46.23	22.70	61.9	46.23
80:20	12.56	62.5	38.52	24.44	37.2	35.77	25.91	43.8	40.73
70:30	8.71	72.3	56.13	19.45	54.8	36.32	17.11	43.8	30.27
50:50	7.88	65.8	36.32	6.28	73.6	56.13	17.34	16.9	22.01
30:70	14.72	53.8	34.67	19.08	11.4	22.01	17.06	31.2	25.32
10:90	22.79	37.2	33.02	10.18	48.0	23.66	16.33	31.2	24.22

3.4 CO_2 absorption

The results of CO_2 absorption test are presented in Figure 11. The test results showed that bottom ash-to-smectite ratios of 90:10, 80:20, and 70:30 showed an initial increase in weight after the first CO_2 injection.

However, in subsequent rounds of gas injection, the sample weight decreased owing to the evaporation of residual moisture, making it impossible to accurately determine the amount of CO_2 absorbed. To address this issue, a modified test was conducted using dried samples to prevent weight loss due to moisture evaporation and to accurately determine CO_2 absorption based on weight increase. To improve the accuracy of CO_2 absorption measurements, dried backfill samples were used to eliminate weight loss caused by moisture evaporation during gas injection. This adjustment revealed that CO_2 uptake increased with higher smectite content, which was consistent with the findings of Franco et al. (2024), who demonstrated enhanced adsorption in silica-pillared smectites with high surface area. Similarly, Mendel (2024) showed that smectite interlayer structures facilitate selective CO_2 adsorption under ambient conditions, reinforcing the mineral's suitability for carbon capture applications. These results confirm that smectite-rich materials possess significant potential for CO_2 sequestration when moisture interference is controlled.

The results of this improved test are shown in Figure 12. The dried backfill material samples were found to absorb carbon dioxide, with the amount of CO_2 absorbed increasing as the proportion of smectite in the sample increased. The CO_2 absorption test conducted on composite backfill materials revealed a clear correlation between smectite content and CO_2 uptake capacity. Specifically, the maximum absorption values for bottom ash-to-smectite ratios of 90:10, 80:20, 70:30, 50:50, 30:70, and 10:90 were 0.78, 0.77, 1.63, 2.01, 3.13, and 3.16 mg/g, respectively. The highest absorption was recorded at the 10:90 ratio (3.16 mg/g), while the lowest occurred at the 80:20 ratio (0.77 mg/g).

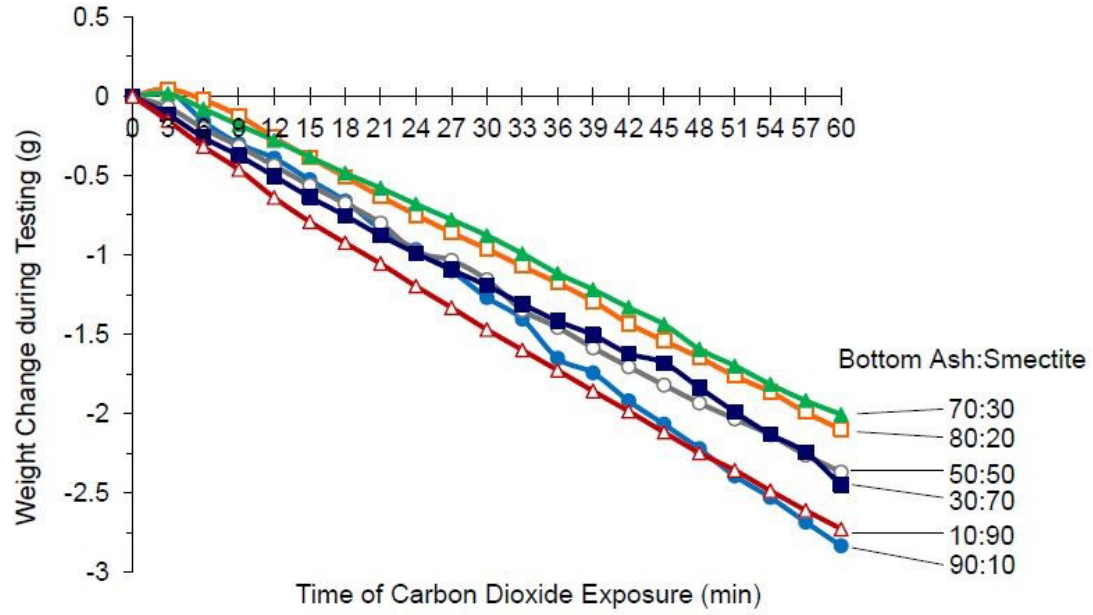

Figure 11. Relationship between weight change during testing and CO_2 exposure duration of the material sample

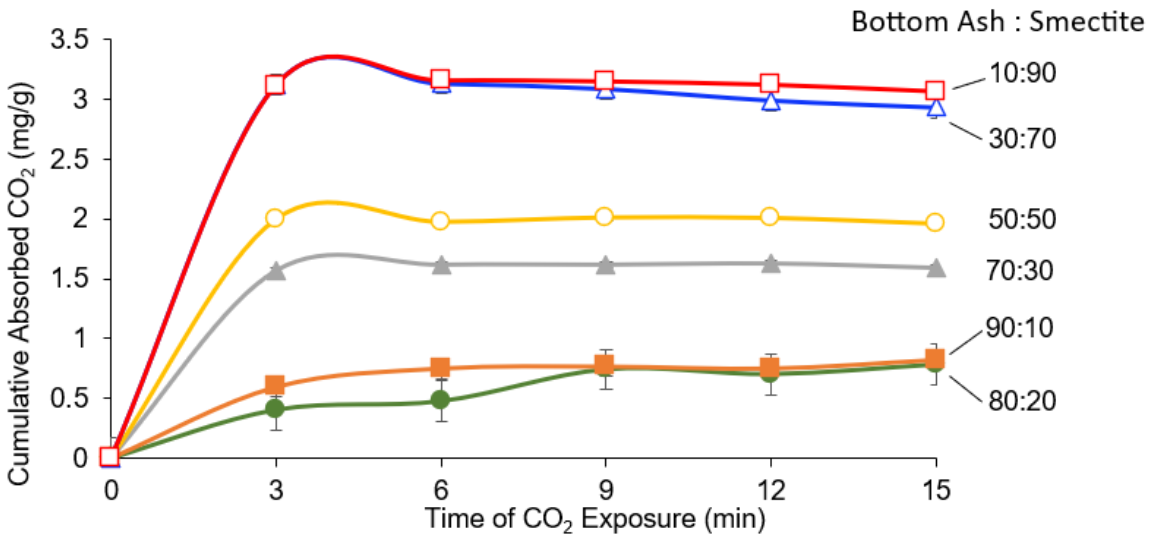

Figure 12. Relationship between CO_2 absorption quantity and exposure duration of the material sample

Figure 13 shows the relationship between bottom ash content (%) and cumulative absorbed CO_2 (Mg/g). The data reveal a strong negative linear correlation, as indicated by the trend line with an R^2 value of 0.9086. This suggests that while smectite enhances CO_2 absorption, increasing bottom ash content reduces this capacity, highlighting a material trade-off that must be considered in optimizing backfill compositions for carbon sequestration. These results underscore the pivotal role of smectite in enhancing CO_2 capture performance. The superior absorption capacity observed in smectite-rich samples can be attributed to the mineral's unique layered structure, composed of stacked thin sheets that offer extensive surface area and interlayer spaces conducive to gas absorption. This structural advantage is supported by the findings of Michels et al. (2015), who demonstrated that smectite exhibits high ion-exchange capacity and a large specific surface area, enabling effective retention of CO_2 molecules. Similarly, Grekov et al. (2020) showed that smectite clays can incorporate CO_2 into their interlayers, particularly when the interlayer spacing is optimized through partial hydration, allowing for enhanced gas entry and retention. However, the limited CO_2 retention observed in certain samples may be due to factors such as the material structure and pore size. If the pore size is too large, gas molecules can easily escape. Additionally, materials with smaller surface areas exhibit lower gas absorption capacities, reducing the overall retention efficiency. Another influencing factor is the high moisture content, which may alter the material structure and affect its ability to trap CO_2. Furthermore, if the interaction force between the gas and material is weak, the CO_2 molecules can easily detach from the material. These findings are consistent with the study by Chouikhi et al. (2019), which investigated the CO_2 absorption properties of different clay minerals. Their research found that natural smectite, could absorb approximately 6 mg CO_2 per gram of mineral.

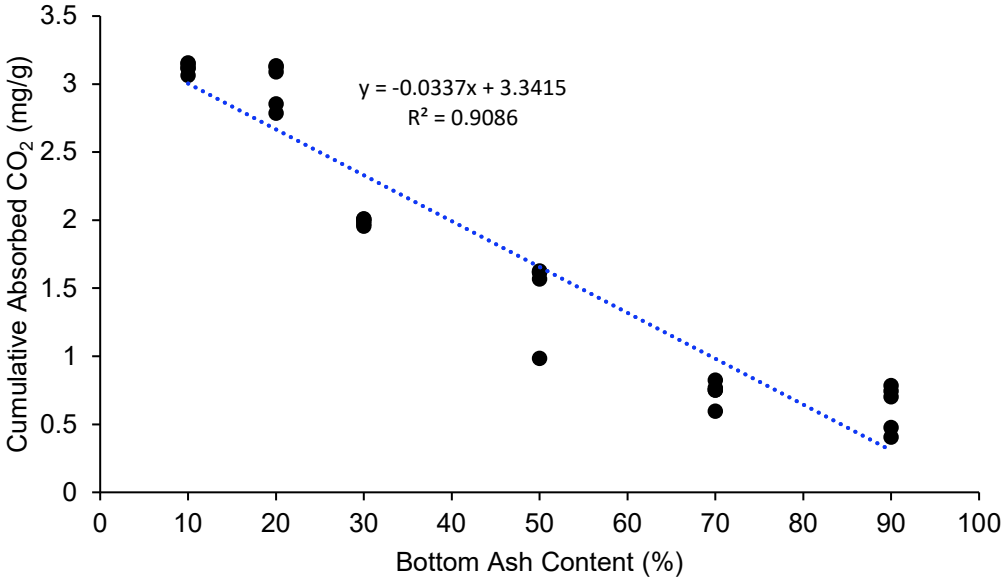

Figure 13. Relationship between bottom ash content and cumulative absorbed CO_2

4. Conclusions

This study explored the potential of bottom ash, a byproduct of coal combustion, as a backfill material for surface coal mines when combined with smectite clay. The research focused on evaluating the mechanical properties and carbon dioxide (CO_2) absorption capacity of bottom ash–smectite mixtures across various ratios and moisture contents.

The specific gravity and moisture content tests of the bottom ash revealed that the dry specific gravity, saturated surface-dry (SSD) specific gravity, apparent specific gravity, and water absorption capacity of the bottom ash were 2.07, 2.33, 2.77, and 12.12%, respectively. In this study, bottom ash with a moisture content of 16.50% was used. Bottom ash and smectite clay were mixed in ratios of 90:10, 80:20, 70:30, 50:50, 30:70, and 10:90, with additional water added at 4%, 7%, and 10%, to perform compaction tests, UCS tests, and CO_2 absorption tests. Compaction tests to determine the optimum moisture content for maximum density revealed that the 50:50 bottom ash-smectite mix with 10% water achieved the highest dry density of 1.57 g/cm³ at an average moisture content of 12.42%. UCS tests for estimating sample cohesion across ratios showed that the 30:70 bottom ash-smectite mix with 10% water exhibited the highest compressive strength of 139 kPa. CO_2 absorption tests to quantify CO_2 uptake capacity demonstrated that the 10:90 bottom ash-smectite mix absorbed the maximum CO_2 at 3.16 mg/g.

The test results indicate that the 50:50 bottom ash-smectite mix achieved the highest dry density, attributed to the coarser particle size and granular texture of bottom ash combined with the finer particles and high cohesion of the smectite. This optimal balance between the two materials enabled superior compaction to be achieved. Conversely, the 10:90 bottom ash-smectite mix exhibited the lowest dry density, as smectite's swelling behavior upon water exposure increased the interstitial voids between particles, reducing the overall density. The 30:70 bottom ash-smectite mix with 10% water content demonstrated the highest UCS. This is because the increased smectite proportion enhances interparticle cohesion, thereby improving the resistance to compressive forces. The 10:90 bottom ash-smectite mix exhibited the highest CO_2 absorption capacity, due to the plate-like layered structure of smectite, which provides a larger reactive surface area for gas absorption. Higher smectite content was directly correlated with enhanced CO_2 sequestration potential.

5. Acknowledgements

This research was made possible through the financial support provided by Prince of Songkla University. The authors would like to express their deepest gratitude to the university for funding this project, which enabled the successful completion and presentation of this work. We would also like to extend our appreciation to Center for Sustainable and Advanced Materials (CSAM), whose guidance and resources contributed significantly to the research process.

6. Authors' Contributions

Pintunicha Pongsena conducted the experimental tests, including unconfined compressive strength analysis and CO_2 absorption experiments, contributed to data interpretation and wrote the manuscript draft.
Matika Buaphian analyzed the experimental data and provided statistical evaluations to support the findings.

Nutdanai Srisuk conducted the experimental tests, including sieve analysis, water content, and compaction test.
Bunlang Mansanit performed material preparation and mixing ratio optimization, ensuring the quality and consistency of the backfill samples.
Manoon Masniyom coordinated project logistics, managed resource allocation, and contributed to manuscript revisions and final editing.
Matthana Khangkhamano handled technical equipment and methodologies for CO_2 absorption measurement and collaborated on result validation.
Naruemol Saoanunt conceived the research concept, developed the study design, and supervised the overall research project.

ORCID
Naruemol Saoanunt https://orcid.org/ 0000-0003-1601-5103

7. Conflicts of Interest

The authors declare no conflict of interest regarding the publication of this article.

References

Ardit, M., Cruciani, G., & Dondi, M. (2012). Local structural relaxation around Co^{2+} along the hardystonite–Co-åkermanite melilite solid solution. *Physics and Chemistry of Minerals, 39*(9), 713-723. https://doi.org/10.1007/s00269-012-0525-9

ASTM. (2007). *Standard test method for particle-size analysis of soils (ASTM D422-63)*. ASTM International. https://doi.org/10.1520/D0422-63R07

ASTM. (2010a). *Standard test method for unconfined compressive strength of cohesive soil (ASTM D2166-06)*. ASTM International. https://doi.org/10.1520/D2166-06

ASTM. (2010b). *Standard practice for classification of soils for engineering purposes (Unified Soil Classification System) (ASTM D2487-06)*. ASTM International. https://doi.org/10.1520/D2487-06

ASTM. (2017). *Standard test method for laboratory determination of water (moisture) content of soil and rock by mass (ASTM D2216-98)*. ASTM International. https://doi.org/10.1520/D2216-98

ASTM. (2020). *Standard test method for direct shear test of soils under consolidated drained conditions (ASTM D3080-11)*. ASTM International. https://doi.org/10.1520/D3080_D3080M-11

ASTM. (2021). *Standard test methods for laboratory compaction characteristics of soil using standard effort (ASTM D698-12)*. ASTM International. https://doi.org/10.1520/D0698-12R21

ASTM. (2023). *Standard test method for relative density (specific gravity) and absorption of fine aggregate (ASTM C128-22)*. ASTM International. https://doi.org/10.1520/C0128-22

Câmara, J. G. D. A., Fraga, T. J. M., Baptisttella, A. M. S., de Araujo, C. M. B., Ferreira, J. M., Sobrinho, M. A. D. M., & de Abreu, C. A. M. (2023). Removal of BTEX and heavy metals from wastewater by modified smectite clays: ion exchange and adsorption mechanisms. *Chemical Papers, 77*, 5519-5529. https://doi.org/10.1007/s11696-023-02882-5

Chouikhi, N., Cecilia, J. A., Vilarrasa-García, E., Besghaier, S., Chlendi, M., Duro, F. I. F., Castellon, E. R., & Bagane, M. (2019). CO_2 adsorption of materials synthesized from clay minerals: A review. *Minerals*, *9*(9), Article 514. https://doi.org/10.3390/min9090514

Franco, F., Cecilia, J. A., Pardo, L., Essih, S., Pozo, M., dos Santos-Gómez, L., & Colodrero, R. M. P. (2024). Reversed Mg-based smectites: A new approach for CO_2 adsorption. *Nanomaterials*, *14*(18), Article 1532. https://doi.org/10.3390/nano14181532

Fujikawa, T., Sato, K., Koga, C., Sakanakura, H., Kubota, H., & Nagayama, Y. (2019). Geotechnical characteristics of carbonated incineration bottom ash using exhaust and CO_2 from waste incineration facilities. *Japanese Geotechnical Society Special Publication*, *9*(4), 130-135. https://doi.org/10.3208/jgssp.v09.cpeg132

Götze, J., & Möckel, R. (2012). *Quartz: Deposits, mineralogy and analytics*. Springer. https://doi.org/10.1007/978-3-642-22161-3

Grekov, D. I., Suzuki-Muresan, T., Kalinichev, G. A., Pré, P., & Grambow, B. (2020). Thermodynamic data of adsorption reveal the entry of CH_4 and CO_2 in a smectite clay interlayer. *Physical Chemistry Chemical Physics, 22*(29), 16727-16733. https://doi.org/10.1039/D0CP02135K

Ingold, P., Weibel, G., Wanner, C., Gimmi, T., & Churakov, S. V. (2024). Hydrological and geochemical properties of bottom ash landfills. *Environmental Earth Sciences, 83*, Article 180. https://doi.org/10.1007/s12665-024-11471-y

Jiarawattananon, M., Wasanapiarnpong, T., & Mongkolkachit, J. (2019). Utilization of lignite bottom ash as a raw material for ceramic tile. *Journal of Metals, Materials and Minerals*, *29*(4), 23-27. https://doi.org/10.14456/jmmm.2019.43

Kim, H.-J., & Lee, H.-K. (2017). Mineral sequestration of carbon dioxide in circulating fluidized bed combustion boiler bottom ash. *Minerals*, *7*(12), Article 237. https://doi.org/10.3390/min7120237

Ksaibati, K., & Sayiri, S. R. K. (2006). *Utilization of Wyoming bottom ash in asphalt mixes*. https://www.ugpti.org/resources/reports/downloads/mpc06-179.pdf

Levien, L., Weidner, D. J., & Prewitt, C. T. (1979). Elasticity of diopside. *Physics and Chemistry of Minerals, 4*, 105-113. https://doi.org/10.1007/BF00307555

Mendel, N. (2024). Smectite-rich clays for CO_2 adsorption and separation [Doctoral dissertation, University of Twente]. https://doi.org/10.3990/1.9789036562119

Michels, L., Fossum, J. O., Rozynek, Z., Hemmen, H., Rustenberg, K., Sobas, P. A., Kalantzopoulos, G. N., Knudsen, K. D., Janek, M., Plivelic, T. S., & da Silva, G. J. (2015). Intercalation and retention of carbon dioxide in a smectite clay promoted by interlayer cations. *Scientific Reports*, *5*, Article 8775. https://doi.org/10.1038/srep08775

Pipatmanomai, S., Fungtammasan, B., & Bhattacharya, S. (2009) Characteristics and composition of lignites and boiler ashes and their relation to slagging: The case of Mae Moh PCC boilers. *Fuel*, *88*(1), 116-123. https://doi.org/10.1016/j.fuel.2008.08.007

Power, M. C. (1953). A new roundness scale for sedimentary particles. *Journal of Sedimentary Petrology, 23*(2), 117-119. https://doi.org/10.1306/D4269567-2B26-11D7-8648000102C1865D

Pusch, R., & Yong, R. N. (2006). *Microstructure of smectite clays and engineering performance*. CRC Press. https://doi.org/10.1201/9781482265675

Scherb, S., Maier, M., Mathias, K., Beuntner, N., & Thienel, K. (2024). Reaction kinetics of calcined smectite in a clinker-free model and a synthetic cement system in comparison with selected calcined phyllosilicates. *Cement and Concrete Research, 189*, Article 10776. https://doi.org/10.1016/j.cemconres.2024.107766

Siddique, R. (2008). *Waste materials and by-products in concrete*. Springer. https://doi.org/10.1007/978-3-540-74294-4

Singh, M., & Siddique, R. (2013). Effect of coal bottom ash as partial replacement of sand on properties of concrete. *Resources, Conservation and Recycling, 72*, 20-32. https://doi.org/10.1016/j.resconrec.2012.12.006

Vishwakarma, K., & Shukla, S. (2024). Bottom ash production, utilization, disposal, and its impact on the environment: A review of state-of-the-art. In G. L. Sivakumar Babu, R. H. Mulangi, & S. Kolathayar (Eds.). *Technologies for sustainable transportation infrastructures* (Vol. 529, pp. 393-406). Springer Nature Singapore. https://doi.org/10.1007/978-981-97-4852-5_31

Wang, P., Shen, X., Qiu, S., Zhang, L., Ma, Y., & Liang, J. (2024). Clay-based materials for heavy metals adsorption: Mechanisms, advancements, and future prospects in environmental remediation. *Crystals, 14*(12), Article 1046. https://doi.org/10.3390/cryst14121046

War, K., Raveendran, G., Roy, S. & Arnepalli, D. N. (2023). Effect of CO_2–clay interaction on swelling stress generation capacity and porosity of clay-rich medium. In *Proceedings of the 9th International Congress on Environmental Geotechnics* (pp. 352-360). https://doi.org/10.53243/ICEG2023-193